Non-Darwinian dynamics in therapy-induced cancer drug resistance

Angela Oliveira Pisco[1,2#], Amy Brock[3#], Joseph Zhou[1,4], Andreas Moor[5], Mitra Mojtahedi[1,4], Dean Jackson[2] and Sui Huang[1,4*]

[1] Institute for Systems Biology, Seattle WA 98109, USA
[2] Faculty of Life Sciences, University of Manchester, Manchester M13 9PT, UK;
[3] Wyss Institute for Biologically Inspired Engineering at Harvard University, Boston, MA 02115, USA;
Present address: Dept of Biomedical Engineering, Institute for Cellular and Molecular Biology, The University of Texas at Austin, Austin 78712, USA;
[4] Institute for Biocomplexity and Informatics, University of Calgary, Alberta AB T2N 1N4, Canada;
[5] Ecole Polytechnique Fédérale de Lausanne, Swiss Institute for Experimental Cancer Research, CH-1015 Lausanne, Switzerland

Supplementary Figures

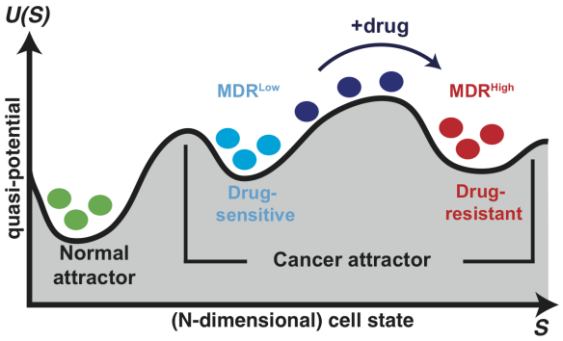

Supplementary Figure S1. Schematic representation of the quasi-potential landscape[61] of epigenetic cell states. Non-genetic acquisition of the MDR^{High} state following entrance into the terrain of unoccupied attractors ("cancer attractor") can be thought of as a state transition between the two (sub)attractors, from the drug-sensitive MDR^{Low} state (blue) to the resistant MDR^{High} state (red). As in such multi-stable systems the transition is noise-driven but modulated by external conditions, including the presence of the drug. Note that by monitoring one dimension of the gene expression state space, e.g., MDR1 expression, we are able to observe cell transition only as a projection (horizontal axis) and do not know what happens in orthogonal (non-observable) dimensions.

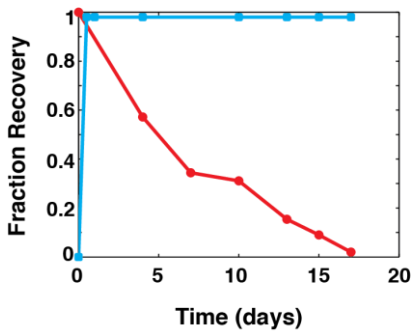

Supplementary Figure S2. Relaxation kinetics. Sorted cells from either subpopulation separately re-establish the "other" subpopulation and reconstitute the original distribution at distinct characteristic rates.

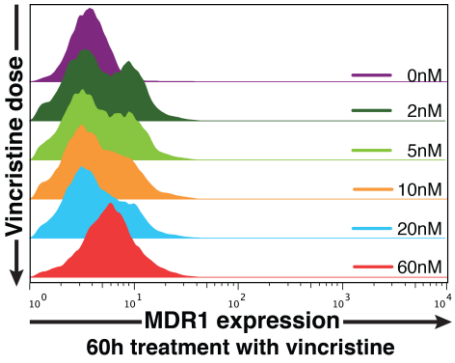

Supplementary Figure S3. Flow cytometry measurements of surface MDR1. Immunostaining for MDR1 shows dose-dependence for the appearance of the MDR1^{High} subpopulation 60 hours after administration of vincristine at the indicated doses

---

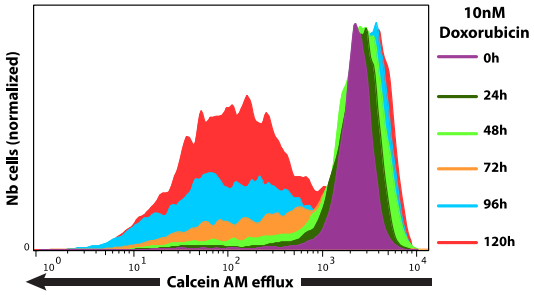

Supplementary Figure S4. Doxorubicin-induced resistant subpopulation. The emergence of a phenotypically distinct, resistant cell population is not specific to treatment of HL-60 cells with the alkaloid drug vincristine but also occurs in a time-dependent manner, with similar kinetics, upon exposure of cells to doxorubicin, a chemotherapeutic agent in the anthracyclin class.

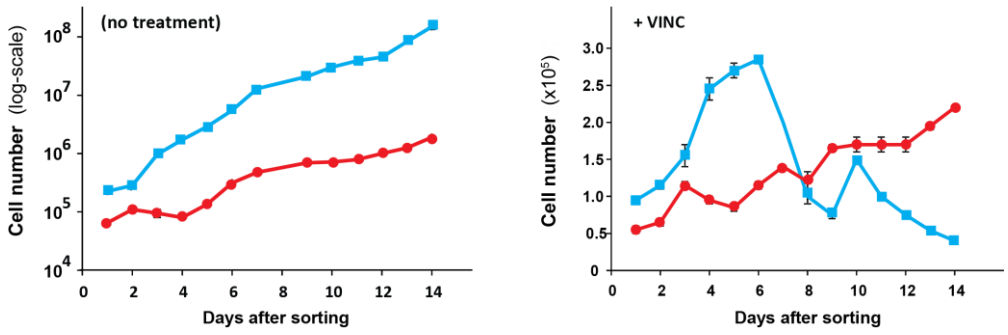

Supplementary Figure S5. Effective growth curves (cell number over time) of the sorted MDR1^{High} and MDR1^{Low} sub-populations in the absence and presence of the drug vincristine (VINC) reveals the protective role of MDR1. Error bars (not visible in all points) indicate spread of technical duplicate measurements in one experiment.

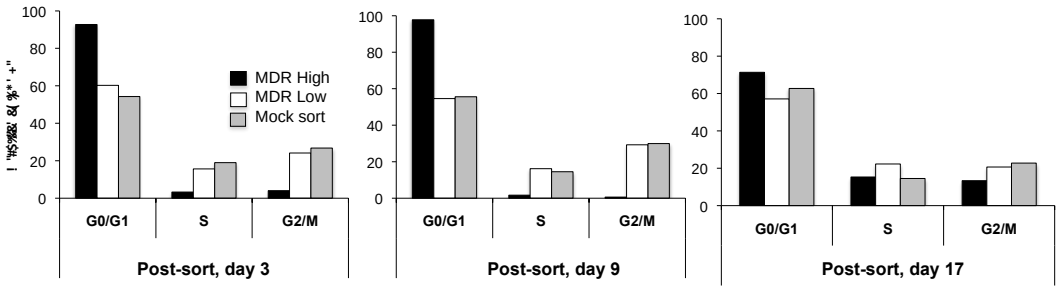

Supplementary Figure S6. Cell cycle analysis of efflux^{High} and efflux^{Low} subpopulations. The proliferation rate of MDR1^{High}/efflux^{High} cells is approximately 50% lower than cells in the MDR1^{Low}/efflux^{Low} state. DRAQ5 staining reveals that MDR1^{High}/efflux^{High} cells are cell cycle arrested and remain so until approximately 17 days post-sorting. As the sorted subpopulations re-equilibrate to similar basal population structure (Fig 1), the difference in cell cycle distribution vanishes. Thus rapid rise of MDR1^{High}/efflux^{High} cells in the population following drug treatment cannot be explained by selection of MDR1^{High}/efflux^{High} cells due to higher proliferation rate. Shown is one representative result of three independent measurements**.**

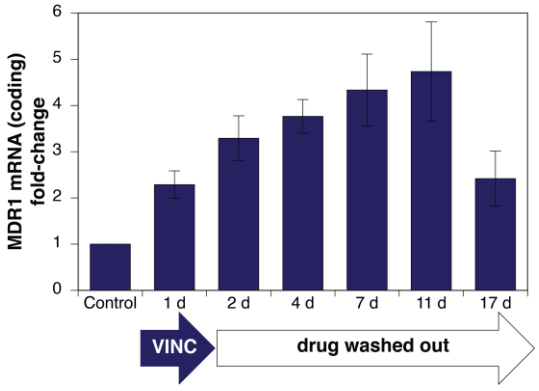

Supplementary Figure S7. Quantitative RT-PCR with primers targeting the coding mRNA of MDR1. Mature MDR1 mRNA levels were measured at the indicated times after drug treatment. Bar height indicate average (*n* = 3 biological replicates) and error bar represent the standard deviation. Technical standard deviations of all shown qPCR Ct-values were < 0.7.

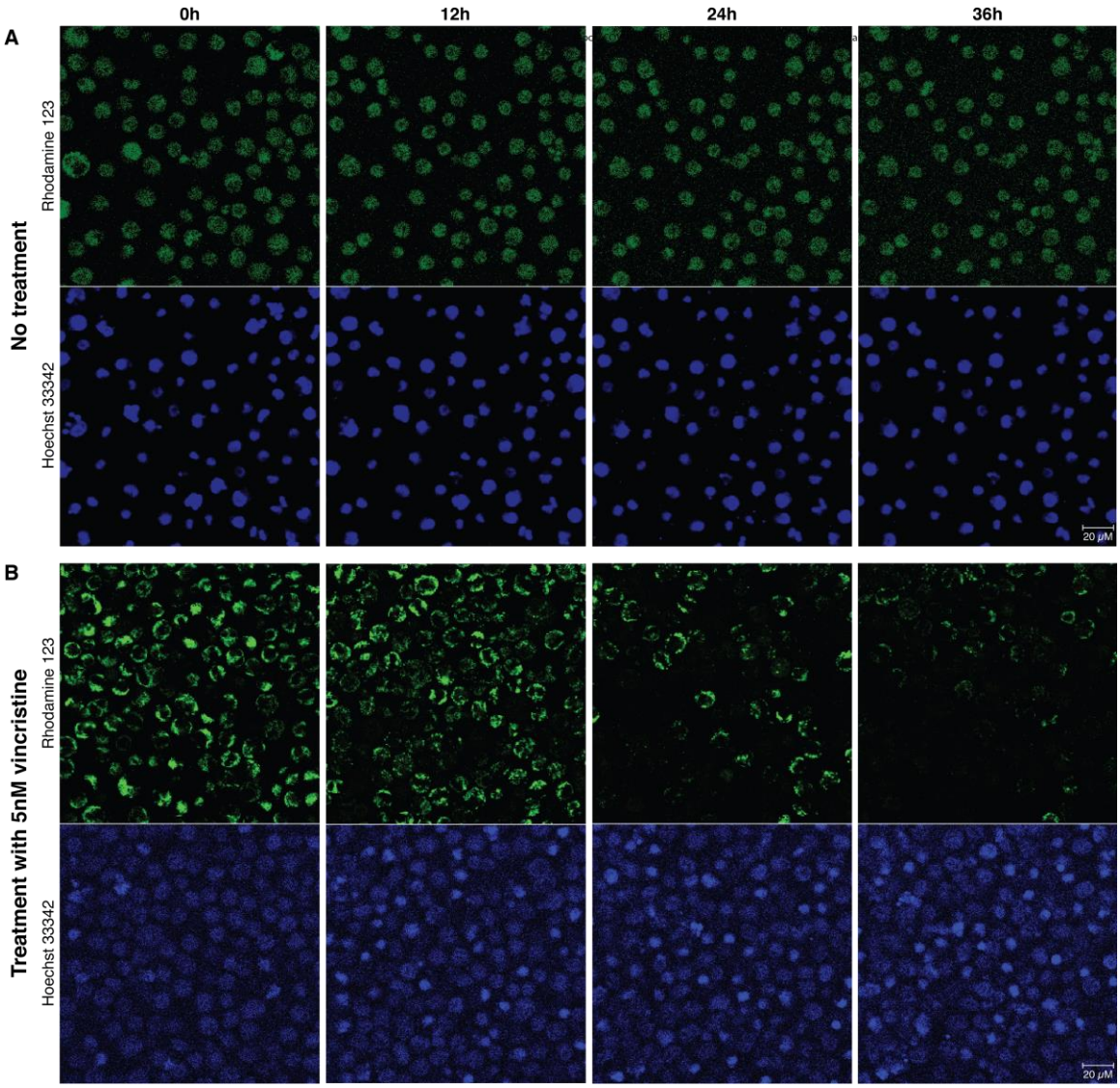

Supplementary Figure S8. Cell-autonomous induction of the MDR phenotype by vincristine. Cells loaded with the fluorescent dye Rhodamine123 (green) as marker of efflux capacity and stained with a DNA dye (Hoechst 33342, blue) as cell indicator and to monitor cell death, were treated with VINC (10nM) (B) and/or vehicle (DMSO) (A) at time *t* = 0h and followed by video microscopy under incubator conditions for 3 days (see online movie for longitudinal tracking of the individual cells). Snapshots at the indicated times are shown. Disappearance of the green fluorescent dye in the viable cells indicates cell autonomous induction of the MDR phenotype. Nuclear condensation in the Hoechst 33342 stain reveals apoptotic cells. As dying cells will eventually release the dye, we quantified only live cells for dye elimination. After 48h monitoring of a typical time-course, 63 % of the live cells treated with VINC exhibited elimination of the dye, representing the switch to the efflux^{High} phenotype compared to 16 % of untreated cells (n=80 cells counted). Scale bar = 20μm. See Supplementary Movies 1 and 2.

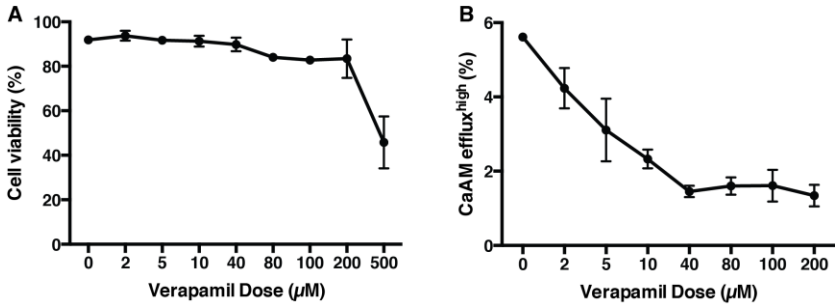

Supplementary Figure S9. Verapamil drug-response in HL60. The cells were incubated 15min with the indicated amounts of verapamil and then washed and stained for CaAM. (A) Viability of cells is minimally affected in the dose range used in the experiments described in the main text. Panel (B) shows that population viability diminished to <80% if more than 40μM of verapamil is used. 10μM of verapamil is enough to reduced basal efflux by ~3-fold. The data shown represents the average of three independent replicates and error bars represent s.d. (Cells used here are a sub-line, a previously selected more resilient HL60 cells that exhibit 6% (instead of 2%) basal MDR activity; this choice was to better quantitate the relative magnitude of inhibition of the pump function).

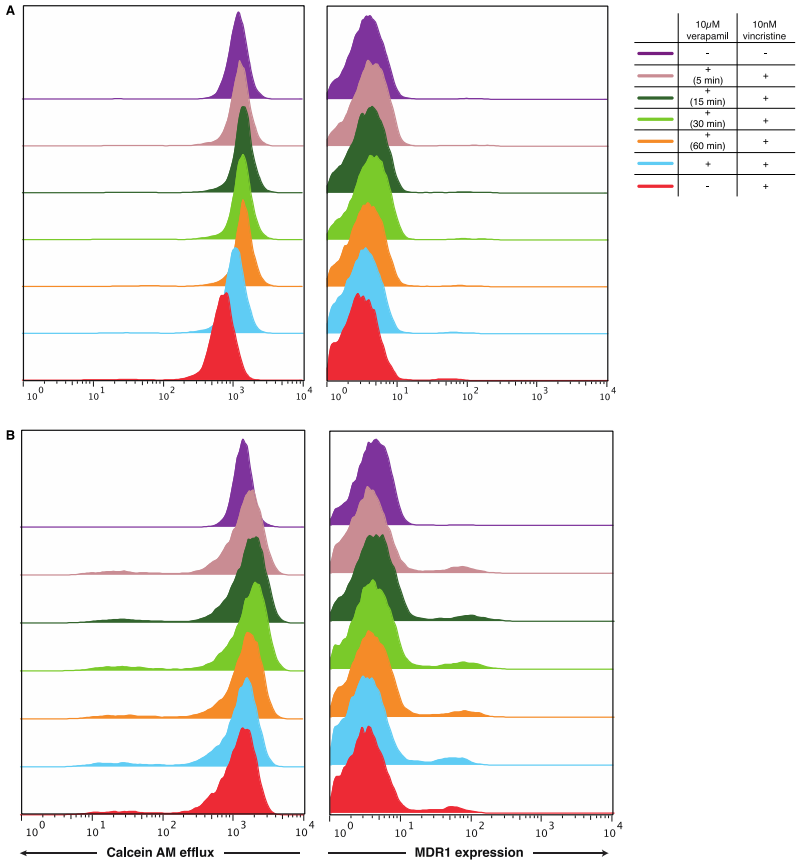

Supplementary Figure S10. Cells induce MDR1 expression independently of the length of pre-incubation with verapamil even after shorter time periods of VINC treatment. The main text (Fig 2D) showed that inhibition of verapamil did not measurably suppress the emergence of the subpopulation of MDR1 expressing cell after 72h. Here we show for completeness sake that this is also the case after 24h (A) and 48h (B) of VINC treatment (the shorter time frame already diminishes the likelihood of selection). The numbers in brackets represent the time delay between verapamil (first) and vincristine (second) adding. For the blue line there was no delay between the adding of the two drugs.

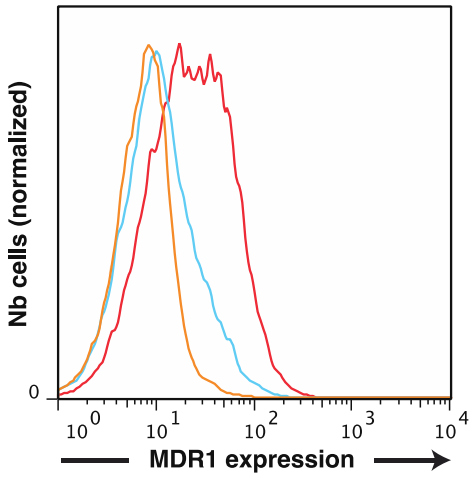

Supplementary Figure S11. Vincristine-exposed cells are primed for faster response upon re-treatment. Previously treated cells for 48h with 10nM vincristine (blue) were re-exposed to vincristine for 72h (red) after a break from the drug ("recovery") of 20 days. Although the expression of MDR1 has almost reverted to that of the untreated control (orange), the transiently treated cells were able to quickly change their status, which allowed them to cope with the presence of drug again without losing viability (see also Fig. 2E).

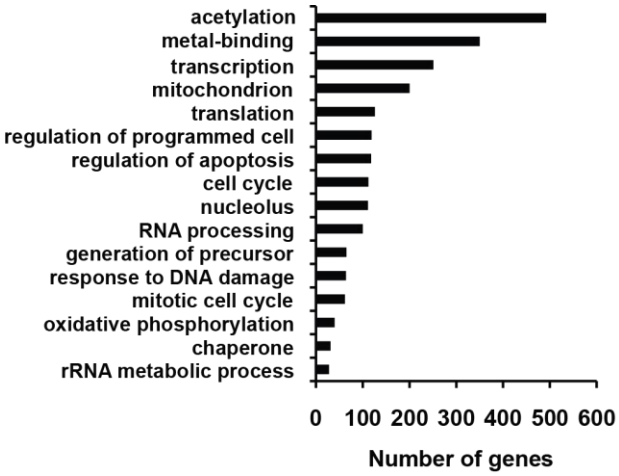

Supplementary Figure S12. Gene Ontology (GO) analysis for enriched functional categories in the differentially expressed genes. The set of 974 genes expressed differentially in the two efflux subpopulations, efflux^{High} and efflux^{Low} that appear 24h after vincristine treatment were tested in DAVID (Database for Annotation, Visualization and Integrated Discovery) against the Homo sapiens gene reference for enrichment of gene ontology categories (for details see Supplementary Table S1). This graph visualizes the distribution of the abundances of the categories that were significantly altered. (Note that this first-pass, crude analysis for enrichment of GO categories is distinct from the 4-way comparison and gene set enrichment analysis shown in Supplementary Fig. S13 and 14 – for details see main text)

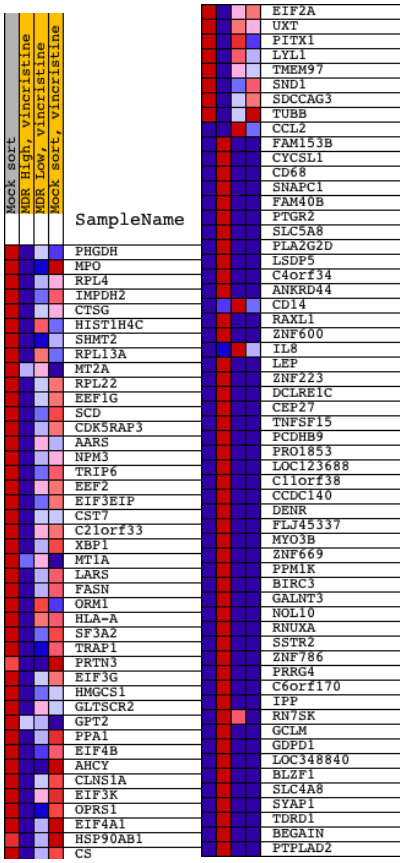

Supplementary Figure S13. GSEA analysis heat map showing the top fifty genes differentially expressed for each phenotype analyzed. The GSEA algorithm examines the differences in expression values and computes if the genes in a gene set are overrepresented at the top or bottom of the ranked list of genes from the expression dataset. The heat map shows the genes in the leading edge subsets and the expression values are represented as colors, where the range of colors (red, pink, light blue, dark blue) shows the range of expression values (high, moderate, low, lowest).

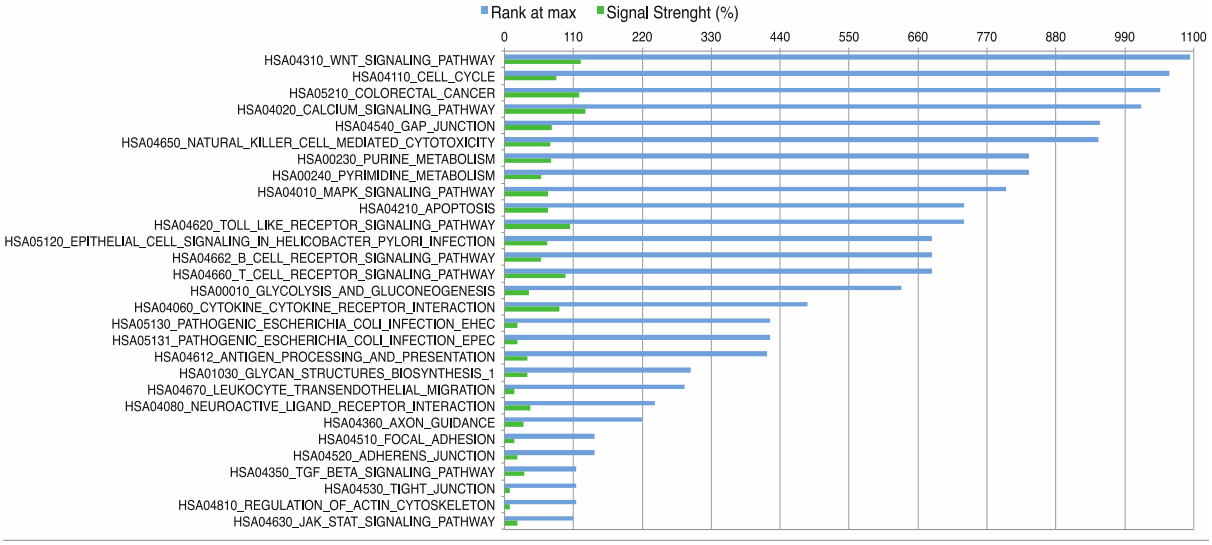

Supplementary Figure S14. Enriched KEGG pathways obtained by GSEA analysis when comparing mock-sorted untreated samples with the other three treated samples. Rank at max, the position in the ranked list at which the maximum enrichment score occurred. Signal strength, the enrichment signal strength resulting from leading edge analysis in GSEA .

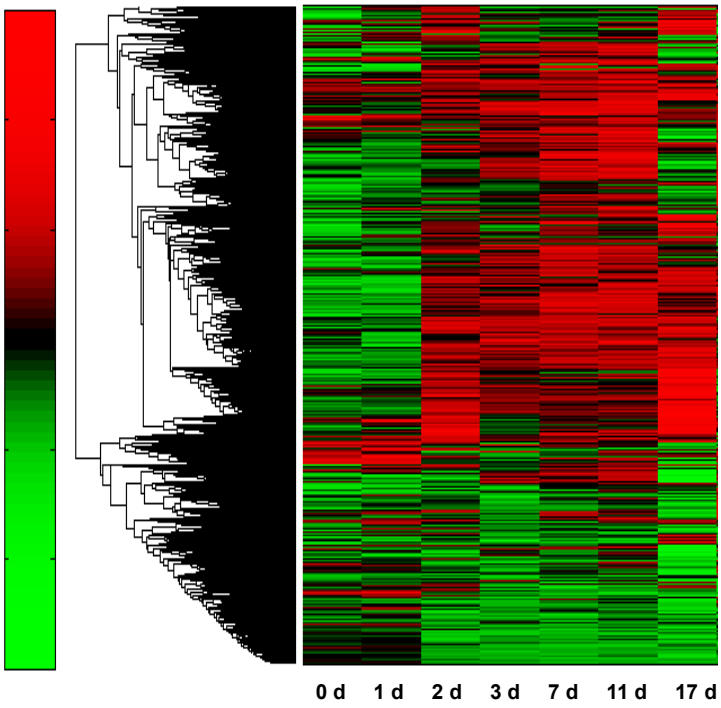

Supplementary Figure S15. A transcriptome-wide gene expression memory effect: classical hierarchical clustering/heat map view of data shown as GEDI maps in Fig. 5. Transient (24h) exposure to vincristine, followed by drug wash-out and continued culture in drug-free media induces gene expression changes that persist longer than 17d. Although MDR1 expression itself returns to baseline in the population by day 17, other dimensions of the gene expression state do not relax to initial levels.

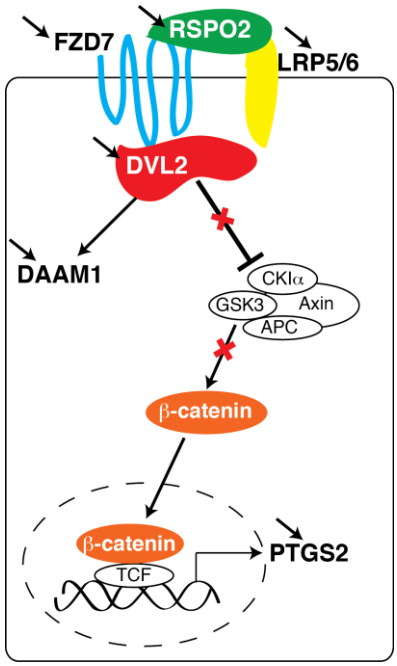

Supplementary Figure S16. Wnt pathway signature from microarray data. Arrows point to those genes whose transcript were increased after treatment of vincristine by at least four fold. APC = adenomatosis polyposis coli, CKIα = casein kinase Iα, DAAM1 = dishevelled associated activator of morphogenesis 1, DVL2 = dishevelled segment polarity protein 2, FZD7= Frizzled 7, GSK3 = glycogen synthase kinase 3, LRP5/6 = low density lipoprotein receptor-related protein 5/6, PTGS2 = prostaglandin-endoperoxide synthase 2, RSPO2 = R-spondin 2, TCF = T cell factor

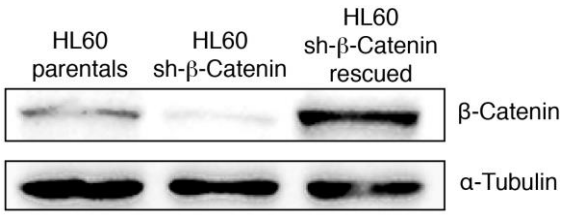

Supplementary Figure S17. Western blot analysis of HL60 cells. Total cell lysates were analyzed to confirm knockdown of β-Catenin. Lanes represent: Parental control, sh-β-Catenin knockdown and sh-resistant β-Catenin rescued knockdown cells. Bands are for β-Catenin (~100 kD band) and α-Tubulin (loading control, ~55 kD).

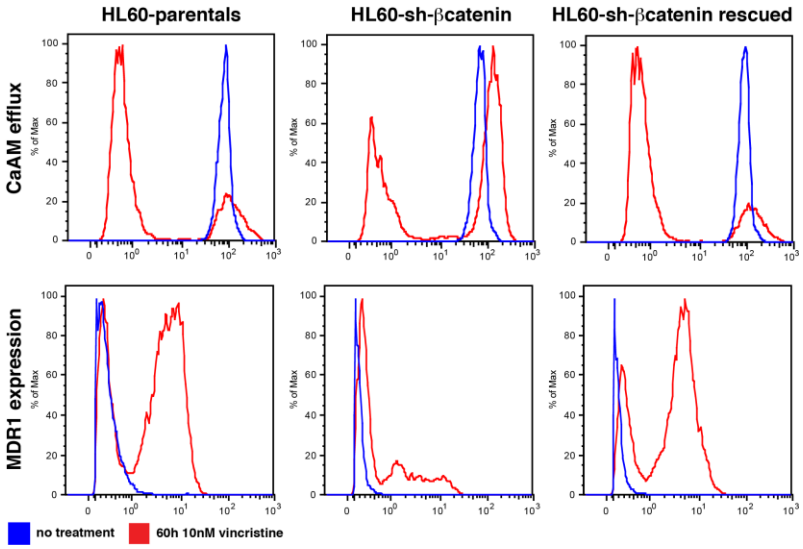

Supplementary Figure S18. Ectopic overexpression of β-catenin completely restored VINC induced efflux and expression of MDR1 in the know-down cells

Supplementary Table

Supplementary Table S1. GO terms analysis with respective p-value associated and the corresponding number of genes. See also Fig. S12**.**

GO term	log(1/P_{val})	# Genes
acetylation	48.62272442	492
metal-binding	3.475957048	350
transcription	3.259699113	251
mitochondrion	16.69359874	200
translation	38.62558904	126
regulation of programmed cell death	3.446641888	119
regulation of apoptosis	3.444060603	118
cell cycle	3.025778422	112
nucleolus	5.567554509	111
RNA processing	6.961395124	100
generation of precursor metabolites and energy	6.561588786	65
response to DNA damage stimulus	3.734892128	64
mitotic cell cycle	3.349026829	62
oxidative phosphorylation	6.862917625	40
chaperone	3.384946712	31
rRNA metabolic process	5.719979196	28